Letter

Testing the fifth force on lepton spins through neutrino oscillations

Rundong Fang,[1,*] Ji-Heng Guo,[1,*] Jia Liu,[2,3,†] and Xiao-Ping Wang[1,4,‡]

[1]*School of Physics, Beihang University, Beijing 100083, China*

[2]*School of Physics and State Key Laboratory of Nuclear Physics and Technology, Peking University, Beijing 100871, China*

[3]*Center for High Energy Physics, Peking University, Beijing 100871, China*

[4]*Beijing Key Laboratory of Advanced Nuclear Materials and Physics, Beihang University, Beijing 100191, China*

(Received 22 November 2024; accepted 19 August 2025; published 3 September 2025)

We investigate a fifth force mediated by a light vector boson that couples to lepton spins, characterized by axial-vector couplings to leptons and vector couplings to nucleons. This interaction generates a potential proportional to the inner product of the lepton spin vector and the nucleon-lepton relative velocity vector, a feature extensively explored with precision spin sensors. Employing weak symmetry, we show that left-handed charged lepton couplings naturally extend to left-handed neutrinos, enabling this fifth force to influence neutrino oscillations. For electron-nucleon couplings, we find that solar and reactor neutrino experiments provide comparable constraints to those from spin sensors and surpass them in the short-range fifth force region. For muon-nucleon couplings, neutrino oscillation experiments exclude the fifth force as a viable explanation for the muon $g-2$ anomaly in the context of a vector mediator, tightening the bounds by 2 orders of magnitude in coupling strength by solar and atmospheric neutrino data. Our results highlight the critical role of neutrino oscillations in probing fifth forces acting across all three generations of lepton spins.

DOI: 10.1103/r9p5-fxzb

Introduction. . Physics beyond the Standard Model (SM) often predicts novel interactions that go beyond the four known fundamental forces, commonly referred to as the "fifth force." Many of these interactions involve the spin of particles [1], and experimental sensitivity can be achieved through spin sensor experiments. These experiments make it possible to measure the fifth force by detecting interactions with either electron spin [2–6] or nucleon spin [7–13].

If the fifth force is mediated by a very light boson, it could operate over long distances. This mediator, typically a scalar or vector particle, couples to nucleons via scalar or vector interactions, and to leptons via pseudoscalar or axial-vector (AV) interactions. As a result, large astronomical bodies, such as the Sun, Earth, and Moon, which contain vast numbers of particles, can serve as sources for this force. In the nonrelativistic limit, they give rise to a potential that is related to charged lepton or nucleon spins [14,15], which can be constrained through precision spin sensor experiments. This opens up the possibility for precision spin sensors to set stringent constraints on the fifth force models [12,16–19].

For a fifth force coupling to lepton spins, weak symmetry suggests that left-handed lepton couplings may extend to left-handed neutrinos. As a result, the same fifth force could influence the evolution of neutrino states as they propagate, allowing neutrino oscillation experiments to serve as tests of this force.

For neutrino oscillations, most prior studies have focused on neutrino nonstandard interactions [20–22], assuming a heavy mediator that generates a potential proportional to local density. A number of works, however, have explored long-range interactions in Refs. [23–34] for the mediator mass less than $\sim 10^{-12}$ eV and Refs. [35,36] for larger mediator mass. These studies generally examine vector-vector (V-V) or scalar-scalar (S-S) interactions, where the primary contributions are spin independent.

In this work, we explore a fifth force mediated by a light vector boson that couples to lepton spins, extending beyond the scalar mediator studied in our previous work [37]. The mediator is characterized by vector and axial-vector (V-AV) couplings to nucleons and leptons, respectively. We demonstrate that this type of fifth force can be tested through neutrino oscillation experiments. For electron-nucleon couplings, both solar and reactor neutrino experiments

*These authors contributed equally to this work.

†Contact author: jialiu@pku.edu.cn

‡Contact author: hcwangxiaoping@buaa.edu.cn

Published by the American Physical Society under the terms of the Creative Commons Attribution 4.0 International license. Further distribution of this work must maintain attribution to the author(s) and the published article's title, journal citation, and DOI. Funded by SCOAP³.

impose stringent and complementary constraints compared to spin sensor experiments and surpass them in the short-range fifth force region. For muon-nucleon couplings, our analysis shows that neutrino oscillations rule out the fifth force explanation for the muon $g-2$ anomaly [38,39] with a vector mediator, tightening the coupling strength constraints by 2 orders of magnitude. Therefore, neutrino oscillations provide a crucial test for the existence of a fifth force acting on lepton spins.

Model setup. We consider a U(1)′ vector gauge boson A' couples to leptons (L) and nucleons (N) through AV and vector couplings, respectively. The general form of its interaction Lagrangian is given by

$$\mathcal{L}_{\rm int} = A'_\mu \left(\boldsymbol{g}_L^{ij} \bar{L}^i \gamma^\mu L^j + \boldsymbol{g}_R^{ij} \bar{e}_R^i \gamma^\mu e_R^j \right) + g_V^N A'_\mu \bar{N} \gamma^\mu N, \quad (1)$$

where i and j are flavor indices and we assume the nucleon couplings are identical for neutrons and protons. Since we require A' coupling to leptons in an AV coupling, therefore, we have

$$\begin{aligned} \mathcal{L}_{\rm int} = {} & \boldsymbol{g}_A^{ij} A'_\mu \left(-\bar{\nu}_L^i \gamma^\mu \nu_L^j + \bar{e}^i \gamma^\mu \gamma^5 e^j \right) \\ & + g_V^N A'_\mu (\bar{p} \gamma^\mu p + \bar{n} \gamma^\mu n), \end{aligned} \quad (2)$$

where $\boldsymbol{g}_A = -\boldsymbol{g}_L = \boldsymbol{g}_R$ ensures that the coupling to leptons is purely axial vector. We assume a flavor-diagonal axial-vector coupling $\boldsymbol{g}_A^{ij} = a_i \delta^{ij}$. To ensure anomaly cancellation, the couplings should satisfy $\sum_i a_i = \sum_i a_i^3 = 0$ [40]. This can be achieved via intergenerational cancellation, e.g., $a_\tau = -a_\mu$, $a_e = 0$, similar to the $L_\mu - L_\tau$ model. However, to stay model independent, we will calculate constraints for one generation at a time.

Fifth force potential. Considering light A', the net baryon charge can behave as electromagnetic (EM) charge and generates the static A' potential. For a point source with net baryon charge of N_n, we can have the generated A' in Yukawa potential as

$$A'_0(\vec{r}) = -g_V^N \frac{N_n}{4\pi r} e^{-m_{A'} r}, \qquad \overrightarrow{A'}(\vec{r}) \simeq 0, \quad (3)$$

where $m_{A'}$ is the mass of A', r is the distance to the point source; the second equality because we assume the source does not have spin polarization. For an extended spherical source, e.g., Earth, with a local number density of nucleons $n(r)$, the static A' potential becomes [32]

$$A'_0(r) = \frac{-g_V^N}{2 m_{A'} r} \int_0^{R_\oplus} dr' n(r') r' \left(e^{-m_{A'}|r'-r|} - e^{-m_{A'}(r+r')} \right), \quad (4)$$

where $R_\oplus$ is the radii of the source. For very light A', $m_{A'} \ll 1/R_\oplus$, one can recover the standard EM potential. For the heavy A' case, $m_{A'} \gg 1/R_\oplus$, one can obtain [32]

$$A'_0(r) \simeq -g_V^N \frac{n(r)}{m_{A'}^2}, \quad (5)$$

by localizing the integral range in Eq. (4) near r, e.g., $r' \in [r - 10 m_{A'}^{-1}, r + 10 m_{A'}^{-1}]$ and neglecting the small exponential suppression factor. Notably, this is similar to the Mikheyev–Smirnov–Wolfenstein (MSW) potential [20,41] as expected.

Neutrino oscillations. The neutrino oscillation probability can be straightforwardly calculated using the following Hamiltonian:

$$\mathcal{H} = U \frac{M^2}{2E_\nu} U^\dagger + V_{\rm MSW} + \boldsymbol{g}_A A'_0, \quad (6)$$

where U is the Pontecorvo-Maki-Nakagawa-Sakata matrix [42,43] and M is the neutrino mass matrix. The second term accounts for the MSW matter effect. The third term introduces the fifth force contribution, arising from A' modifying the neutrino momentum as, $p_\mu \to p_\mu - \boldsymbol{g}_A A'_\mu$ [37,44,45]. In the following analysis, we focus on the diagonal couplings $\boldsymbol{g}_A^{ee}$ and $\boldsymbol{g}_A^{\mu\mu}$, while generalizations to other couplings can be readily performed. The oscillation probabilities are computed through comprehensive numerical simulations with Hamiltonian (6). We analyze across various neutrino experiments, including accelerator and reactor long-baseline (LBL) experiments, reactor medium-baseline (MBL) experiments, atmospheric neutrino (ATM) experiments, and solar neutrino (Solar) experiments.

For the reactor and accelerator experiments, we assume a constant interaction Hamiltonian $\Delta\mathcal{H}$ during propagation, taking Earth matter density as 2.7 g/cm^3 for MSW effects. For ATM neutrinos, we incorporate the variable Earth matter density along the neutrino's path, segmenting the trajectory to calculate oscillation probability using PREM density data [46]. The production height of atmospheric neutrinos is fixed at 10 km above the Earth surface. For solar neutrinos, we calculate the oscillation probability following [47,48], with the solar nucleon density from GS98 data [49]. Details of our numerical methods can be found in our previous work [37].

In Fig. 1, we illustrate the oscillation probability ratios between scenarios with and without the fifth force effect across different types of neutrino experiments. The left panel shows the survival probability ratio for LBL experiments as a function of E_ν and L, with parameters $g_A^{\mu\mu} \neq 0$, $m_{A'} = 10^{-14}$ eV, and $g_A^{\mu\mu} g_V^N = -10^{-48}$. The central panel presents the oscillation ratio for ATM in terms of E_ν and $\cos\theta$, with $m_{A'} = 10^{-14}$ eV and $g_A^{\mu\mu} g_V^N = -10^{-50}$. The right panel displays the survival probability ratio for Solar as a function of E_ν and $g_A^{\mu\mu} g_V^N$ at a production location of $r = 0.05 R_\odot$ and $m_{A'} = 10^{-17}$ eV $> 1/R_\odot$, with $R_\odot$ the radii of the Sun.

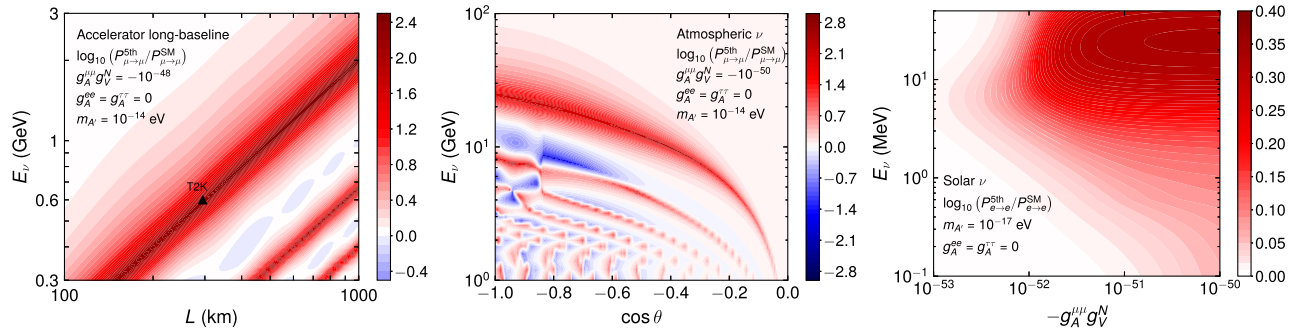


FIG. 1. The contour plots of ratios between the oscillation probability with and without the fifth force. Left panel: the ν_μ survival probability ratio as a function of neutrino energy E_ν and baseline length L, with the black triangle marking the typical neutrino energy and baseline for the T2K experiment. Central panel: the ν_μ survival probability ratio as a function of E_ν and $\cos\theta$, relevant for IceCube experiments. Right panel: the solar neutrino disappearance probability ratio as a function of E_ν and the coupling $g_A g_V^N$.

In both the left and central panels of Fig. 1, the ratios display asymptotic behavior at high neutrino energies. In this limit, the vacuum oscillation term becomes small compared to the MSW potential and the fifth force potential. For large values of the product $g_A^{\mu\mu}g_V^N$, the full Hamiltonian contains large contributions in the 11 and 22 terms, which suppresses $\nu_\mu \to \nu_e$ and $\nu_\mu \to \nu_\tau$ oscillations, resulting in a nearly unchanged survival probability $P^{5th}_{\mu\mu}$. In contrast, without the fifth force, $\nu_\mu \to \nu_\tau$ oscillations remain significant, consistent with the SM. Thus, the asymptotic lines in the left and central panels correspond to the minimum probability for two-flavor $\nu_\mu \to \nu_\tau$ oscillations in the SM scenario. For solar neutrinos in the right panel of Fig. 1, the fifth force effect depends on both the coupling strength and neutrino energy. Stronger couplings and higher energies lead to more significant deviations from SM predictions. For reactor LBL and MBL experiments, we provide probability ratio plots in the Supplemental Material [50].

Analysis. After numerically calculating the transition and survival probabilities, we analyze various neutrino oscillation data to constrain the fifth force couplings.

For ATM neutrinos, we consider the Icecube DeepCore [51–54] which provides the 1-D events distribution respect to the neutrino energy E_ν, the cosine zenith angle $\cos\theta$, and the L/E_ν ratio [54]. To analyze the sensitivity of atmospheric neutrino data to the fifth force, we apply the χ^2 method [55,56], defined as

$$\chi^2(N,O) = 2\sum_\alpha \left(N_\alpha - O_\alpha + O_\alpha \ln\frac{O_\alpha}{N_\alpha}\right), \tag{7}$$

where N and O are the expected and observed number of events, respectively, and the index α represents the bin indices for the events distribution given by the experiment. To calculate the expected number of events in the fifth force model, we divide E and $\cos\theta$ into small 2-D bins. For each bin, the ratio of events in the fifth force model (N_{ij}) to those in the SM (N^0_{ij}) is given by

$$\frac{N_{ij}}{N^0_{ij}} = \frac{\sum_a \iint_{ij} P_{a\to\mu/\bar{\mu}}\Phi_a dE d\cos\theta}{\sum_a \iint_{ij} P^0_{a\to\mu/\bar{\mu}}\Phi_a dE d\cos\theta}, \tag{8}$$

where i and j represent the bin indices for E and $\cos\theta$, $P_{a\to\mu/\bar{\mu}}$ is the neutrino oscillation probability for the fifth force model, $\Phi_a(E_\nu,\cos\theta)$ is the ATM neutrino flux at its production location before the oscillation process provided by [57], and a sums over e, μ neutrinos and antineutrinos. Using Eq. (8), we rescale the SM event distribution to obtain the event distribution under the fifth force model.

For accelerator LBL neutrinos, we analyze data from T2K [58,59], which uses Super-Kamiokande [60] as its far detector, located 295 km from the source. The detector is a large water Cherenkov device with a fiducial volume of 22.5 ktons. The near detector complex (ND280) is located 280 m from the source. The neutrino beam, produced by a proton beam dump, peaks at ∼0.6 GeV, as shown as the black triangle point in Fig. 1. For the fifth force model, the expected number of events is rescaled using Eq. (8), with the oscillation probability now depending only on neutrino energy E_ν due to the fixed baseline. The χ^2 statistic is given by

$$\chi^2 = \sum_i \frac{(N_i - O_i)^2}{(\delta O_i)^2}, \tag{9}$$

where δO_i is the uncertainty of the observed signals in the ith bin. Observed and expected ν_μ and $\bar{\nu}_\mu$ event rates and the neutrino parameters θ_{23} and Δm^2_{23} are taken from Ref. [59].

For solar neutrinos, we use the data from BOREXINO [61], SNO + SK [62], and calculate the χ^2 as

$$\chi^2 = \sum_i \frac{(P_{ee}(E_i) - P^{obs}_{ee}(E_i))^2}{(\delta P^{obs}_{ee}(E_i))^2}, \tag{10}$$

where $P_{ee}(E_i)$ is the theoretical survival probability of electron neutrinos at energy E_i, and $P_{ee}^{\rm obs}(E_i)$ and $\delta P_{ee}^{\rm obs}(E_i)$ are the observed survival probability and its uncertainty. Observed values from BOREXINO [61] include: $P_{ee}^{\rm obs}$ for pp neutrinos at 0.267 MeV is 0.57 ± 0.09, for ^{7}Be neutrinos at 0.862 MeV is 0.53 ± 0.05, and for pep neutrinos at 1.44 MeV is 0.43 ± 0.11. For high-energy region ^{8}B neutrinos, data points include: at 8.1 MeV, 0.37 ± 0.08; at 7.4 MeV, 0.39 ± 0.09; and at 9.7 MeV, 0.35 ± 0.09. The SNO + SK [62] analysis provides a survival probability at 10 MeV(^{8}Bneutrinos) of 0.308 ± 0.015, with very small uncertainty. These data, particularly the SNO + SK results, dominate the sensitivity to $g_A^{ee} g_V^N$ and $g_A^{\mu\mu} g_V^N$ due to their relevance at high energies, shown in Fig. 1.

For reactor experiments, we use data from KamLAND [63–66] and Daya Bay [67–70]. Since the analyses are similar and their constraints are weaker than the solar, ATM, and accelerator neutrino results, we postpone the details of analysis until the Supplemental Material [50].

Muon $g-2$. External fields generated by dark matter [71,72] or fifth forces [37–39,73] may couple to muon spins, providing a testable signature in storage ring experiments and offering a potential solution to the muon $g-2$ anomaly [37,39].

If A' has the $g_A^{\mu\mu}$ coupling, it contributes to $(g-2)_\mu$. In order to calculate its contribution, we boost the muon to its rotation muon rest frame (RMRF), where the muon is at rest [71,72]. The fifth force Hamiltonian in RMRF is then given by [14,15]

$$H_{\rm 5th} = g_A^{\mu\mu} \hat{\vec{\sigma}} \cdot \vec{\tilde{A}}' = -g_A^{\mu\mu} \hat{\vec{\sigma}} \cdot \frac{\vec{p}}{m_\mu} A_0', \tag{11}$$

where $\vec{p}$ is the momentum of muon in the lab frame, $\tilde{A}'_\alpha \approx (\gamma A_0', -\gamma\vec{\beta} A_0')$ is the A' field in RMRF, $\gamma \approx 29.3$ and $\vec{\beta}$ are the boost factor and velocity of the muon, respectively. Using the spin evolution relations [37,73],

$$\frac{d\vec{S}}{dt} = \vec{\omega} \times \vec{S}, \qquad \frac{d\hat{S}_i}{dt} = i\big[H, \hat{S}_i\big], \tag{12}$$

where $\hat{S}_i = \hat{\sigma}_i/2$ is the muon spin operator. We have the precession frequency from the fifth force contribution:

$$\delta\vec{\omega} = -2 g_A^{\mu\mu} \frac{\vec{p}}{m_\mu} A_0'. \tag{13}$$

Since $\vec{p} \perp \vec{\omega}$, the precession frequency shift is [71,72]

$$\Delta\omega = \sqrt{(\delta\vec{\omega} + \vec{\omega})^2} - |\vec{\omega}| \approx |\delta\vec{\omega}|^2/(2|\vec{\omega}|). \tag{14}$$

Notably, $\Delta\omega$ is independent of the sign of the coupling constant $g_A^{\mu\mu} g_V^N$. In RMRF, we have $|\vec{\omega}| = \gamma\omega_a \equiv \gamma(\omega_c - \omega_s)$, where ω_c (ω_s) is the cyclotron (spin precession) frequency in the lab frame. In RMRF, using Eqs. (13) and (14), we have

$$\Delta\omega = \frac{2 g_A^2 (\gamma^2 - 1) A_0'^2}{\gamma\omega_a}. \tag{15}$$

Back to the lab frame, $\Delta\omega_{\rm lab} = \Delta\omega/\gamma$. The relative frequency shift connects to the muon $g-2$ as $\Delta\omega_{\rm lab}/\omega_a \approx \Delta a_\mu/a_\mu$ [39,74,75]. Given the recent result $\Delta a_\mu = (249 \pm 48) \times 10^{-11} > 0$ [74,76–78], we find that, for $m_{A'} = 10^{-14}$ eV, the coupling range $|g_A^{\mu\mu} g_V^N| \in [7.2 \times 10^{-50}, 1.4 \times 10^{-49}]$ can fit the current muon $g-2$ anomaly at 3σ. Coupling larger than 1.4×10^{-49} is excluded. Constraints for other A' mass can be rescaled accordingly, with the results displayed as yellow grid regions in Fig. 2.

Precision spin sensors. Laboratory experiments utilizing precision spin sensors can also probe $g_A^{ee} g_V^N$ couplings. In the nonrelativistic limit, the Hamiltonian (11) can generate a spin-velocity dependent potential [14,15]:

$$V_{12+13} = g_A^{ee} g_V^N \vec{\sigma}_e \cdot \vec{v}_{\rm rel} \frac{1}{4\pi r} e^{-m_{A'} r}, \tag{16}$$

where $\vec{\sigma}$ is the Pauli matrices for electrons, $\vec{v}_{\rm rel}$ and r are the relative velocity and distance between electrons and nucleons.

For a very light mediator, the most relevant experiment is the torsion pendulum by Heckel *et al.* [16]. This setup uses a spin pendulum made of AlNiCo and $SmCo_5$, materials with a significant number of polarized electrons. When an external field $\vec{\beta}$ couples to the spin, it contributes to the pendulum's energy as $E_p = -N_p \vec{\sigma}_p \cdot \vec{\beta}$, where $N_p \sim 10^{23}$ is the net number of polarized spins, and $\vec{\sigma}_p$ represents the pendulum's spin orientation. This interaction produces a measurable torque $\vec{\tau} = N_p \vec{\sigma}_p \times \vec{\beta}$. For a fifth force range $\lambda \equiv m_{A'}^{-1} \gg 1.5 \times 10^{11}$ m (Sun) and 4×10^8 m (Moon), limits are set at $g_A^{ee} g_V^N$ values of $(+0.2 \pm 1.2) \times 10^{-56}$ and $(-3.1 \pm 2.4) \times 10^{-50}$, shown as solid gray lines in Fig. 2.

Clayburn 2023 [19] considered Earth as a moving, unpolarized source, where particles within Earth have velocities different from electrons on the surface, thus, creating the potential V_{12+13}. By analyzing various electron and nuclear spin sensors, they established bounds on orientation-dependent energy shifts. The Heckel torsion-pendulum result led to a new constraint of $|g_A^{ee} g_V^N| < 10^{-52}$ for a force range $\lambda > R_{\rm Earth}$, surpassing Heckel's old result [16] for $\lambda \lesssim 10^{10}$ m. For smaller force ranges $\lambda < R_{\rm Earth}$, the constraint is $\propto \lambda^{-3}$ from the volume integration of Eq. (16). Note $v_{\rm rel}$ is proportional to r, thus canceling r in the denominator. For $\lambda < 100$ m, density inhomogeneities near the detector limit experimental accuracy, which is the vertical gray dotted line in Fig. 2.

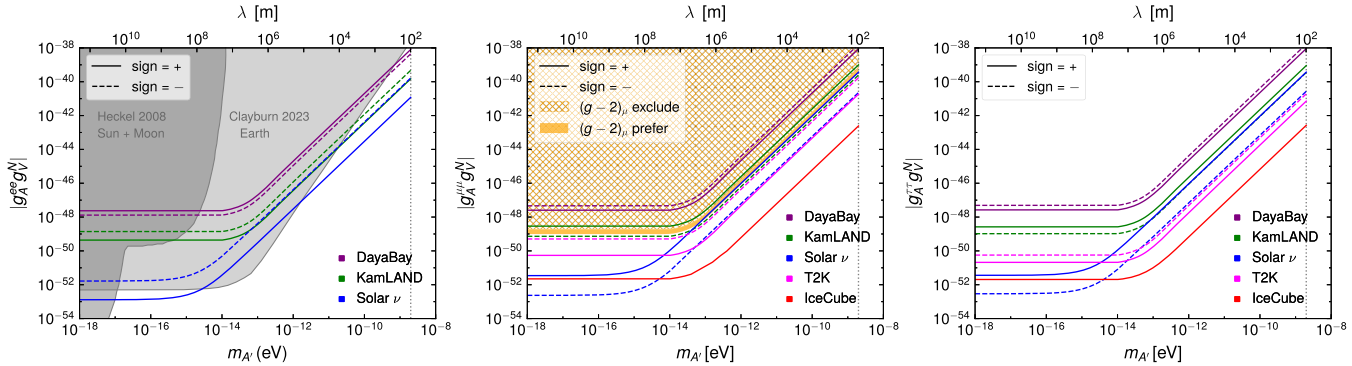


FIG. 2. The 95% CL constraints on the fifth force model with electron (left), muon (center), and tau (right) couplings. The lines show constraints from reactor experiments (Daya Bay [67–70], KamLAND [63,64]), solar neutrino experiments (BOREXINO [61], SNO [79], SK [80,81]), the accelerator experiment T2K [58,59], and atmospheric neutrino data from IceCube DeepCore [51,53,54]. Solid (dashed) lines represent positive (negative) values of the coupling constant $g_A g_V^N$. The red dashed curve is omitted as the IceCube constraints for positive and negative couplings are nearly identical. The existing constraints from spin-sensor experiments are shown in gray, labeled as Heckel 2008 [16] and Clayburn 2023 [19]. The orange hatched region (shaded region) shows parameter space excluded (preferred) by current muon $g-2$ measurements [74,76–78].

Results. We display constraints from various neutrino experiments using the χ^2 analysis in Fig. 2. With two free parameters, $m_{A'}$ and $g_A g_V^N$, the 95% confidence level corresponds to $\Delta\chi^2 = 5.99$. Because of potential inhomogeneities in Earth's local density, we consider only parameter space where $\lambda \equiv 1/m_{A'} > 100$ m [19].

For $g_A^{ee} g_V^N$ couplings, the primary constraint arises from solar neutrino experiments, which limit $g_A^{ee} g_V^N$ to $[-16.5, 1.3] \times 10^{-53}$ in the massless limit and $[-41.6, 3.0] \times 10^{-50} \times m_{A'}^2/(10^{-13}\ \text{eV})^2$ in the high-mass region. For positive $g_A^{ee} g_V^N$, solar neutrino limits are stronger than those from the Clayburn 2023 study [19]. In the high-mass range, neutrino oscillation constraints scale as $m_{A'}^{-2}$ [see Eq. (5)], while spin-sensor constraints scale as $m_{A'}^{-3}$, making neutrino oscillations more sensitive for $\lambda \lesssim 10^5$ m. The reactor experiments KamLAND and Daya Bay provide constraints of $[-13.9, 4.3] \times 10^{-50}$ and $[-1.3, 2.3] \times 10^{-48}$ in the massless limit.

Solar neutrinos yield stronger constraints than reactor neutrinos due to the higher nucleon density and total mass of Sun and the higher energy of ^{8}B neutrinos compared to reactor neutrinos. Additionally, solar constraints vary by an order of magnitude between positive and negative $g_A^{ee} g_V^N$ values, as negative values fit solar data better than the SM [82].

For $g_A^{\mu\mu} g_V^N$ couplings, the strongest constraints come from ATM neutrino experiments using IceCube data, due to the high neutrino energy. These constraints are $|g_A^{\mu\mu} g_V^N| < 1.2 \times 10^{-51} \times m_{A'}^2/(10^{-13}\ \text{eV})^2$ at high masses and $|g_A^{\mu\mu} g_V^N| < 2.2 \times 10^{-52}$ in the massless limit. Solar neutrino and accelerator (T2K) experiments also impose strong constraints, with notable sign dependencies for $g_A^{\mu\mu} g_V^N$, which are not observed in the IceCube results. Typically, if a positive $g_A^{ee} g_V^N$ provides a stronger constraint than the negative, the reverse is true for $g_A^{\mu\mu} g_V^N$ in the same experiment. Our analysis shows that solar, ATM, and accelerator neutrino experiments exclude the fifth force parameter space for $g_A^{\mu\mu} g_V^N$ relevant to the muon $g-2$ anomaly. For $g_A^{\tau\tau} g_V^N$ couplings, the results are similar to $g_A^{\mu\mu} g_V^N$ couplings.

Discussions. We examined a fifth force model with lepton spin couplings mediated by a vector boson, using neutrino oscillation experiments as a probe. Our results reveal that neutrino experiments provide constraints on electron-nucleon couplings comparable to those from precision spin sensors, outperforming them in the high-mass region. For muon-nucleon couplings, neutrino oscillations yield constraints 2 orders of magnitude stronger than those from muon $g-2$ measurements. Tau-nucleon couplings are constrained by neutrino oscillations at a similar level to muon couplings. Our work highlights the capability of neutrino experiments to probe fifth force interactions across all three lepton generations.

Acknowledgments. The work of J. L. is supported by the National Science Foundation of China under Grants No. 12475103, No. 12235001, and No. 12075005. The work of X. P. W. is supported by the National Science Foundation of China under Grant No. 12375095 and the Fundamental Research Funds for the Central Universities.

[1] L. Cong *et al.*, Spin-dependent exotic interactions, Rev. Mod. Phys. **97**, 025005 (2025).

[2] W.-T. Ni, S.-S. Pan, H.-C. Yeh, L.-S. Hou, and J.-L. Wan, Search for an axionlike spin coupling using a paramagnetic salt with a dc SQUID, Phys. Rev. Lett. **82**, 2439 (1999).

[3] P. H. Chu, E. Weisman, C. Y. Liu, and J. C. Long, Search for exotic short-range interactions using paramagnetic insulators, Phys. Rev. D **91**, 102006 (2015).

[4] N. Crescini, G. Carugno, P. Falferi, A. Ortolan, G. Ruoso, and C. C. Speake, Search of spin-dependent fifth forces with precision magnetometry, Phys. Rev. D **105**, 022007 (2022).

[5] P. V. Vorobev and Y. I. Gitarts, A new limit on the arion interaction constant, Phys. Lett. B **208**, 146 (1988).

[6] Y. Huang *et al.*, New constraints on exotic spin-spin-velocity-dependent interactions with solid-state quantum sensors, Phys. Rev. Lett. **132**, 180801 (2024).

[7] B. J. Venema, P. K. Majumder, S. K. Lamoreaux, B. R. Heckel, and E. N. Fortson, Search for a coupling of the Earth's gravitational field to nuclear spins in atomic mercury, Phys. Rev. Lett. **68**, 135 (1992).

[8] A. G. Glenday, C. E. Cramer, D. F. Phillips, and R. L. Walsworth, Limits on anomalous spin-spin couplings between neutrons, Phys. Rev. Lett. **101**, 261801 (2008).

[9] G. Vasilakis, J. M. Brown, T. W. Kornack, and M. V. Romalis, Limits on new long range nuclear spin-dependent forces set with a K—He-3 co-magnetometer, Phys. Rev. Lett. **103**, 261801 (2009).

[10] H. Su, Y. Wang, M. Jiang, W. Ji, P. Fadeev, D. Hu, X. Peng, and D. Budker, Search for exotic spin-dependent interactions with a spin-based amplifier, Sci. Adv. **7**, abi9535 (2021).

[11] K. Tullney *et al.*, Constraints on spin-dependent short-range interaction between nucleons, Phys. Rev. Lett. **111**, 100801 (2013).

[12] K. Wei, W. Ji, C. Fu, A. Wickenbrock, V. V. Flambaum, J. Fang, and D. Budker, Constraints on exotic spin-velocity-dependent interactions, Nat. Commun. **13**, 7387 (2022).

[13] S. Zhang, Z.-L. Ba, D.-H. Ning, N.-F. Zhai, Z.-T. Lu, and D. Sheng, Search for spin-dependent gravitational interactions at earth range, Phys. Rev. Lett. **130**, 201401 (2023).

[14] B. A. Dobrescu and I. Mocioiu, Spin-dependent macroscopic forces from new particle exchange, J. High Energy Phys. 11 (2006) 005.

[15] P. Fadeev, Y. V. Stadnik, F. Ficek, M. G. Kozlov, V. V. Flambaum, and D. Budker, Revisiting spin-dependent forces mediated by new bosons: Potentials in the coordinate-space representation for macroscopic- and atomic-scale experiments, Phys. Rev. A **99**, 022113 (2019).

[16] B. R. Heckel, E. G. Adelberger, C. E. Cramer, T. S. Cook, S. Schlamminger, and U. Schmidt, Preferred-frame and *CP*-violation tests with polarized electrons, Phys. Rev. D **78**, 092006 (2008).

[17] H. Yan, G. A. Sun, S. M. Peng, Y. Zhang, C. Fu, H. Guo, and B. Q. Liu, Probe spin-velocity dependent new interactions by spin relaxation times of polarized ^3He gas, Phys. Rev. Lett. **115**, 182001 (2015).

[18] L. Y. Wu, K. Y. Zhang, M. Peng, J. Gong, and H. Yan, New limits on exotic spin-dependent interactions at astronomical distances, Phys. Rev. Lett. **131**, 091002 (2023).

[19] N. B. Clayburn and L. R. Hunter, Using Earth to search for long-range spin-velocity interactions, Phys. Rev. D **108**, L051701 (2023).

[20] L. Wolfenstein, Neutrino oscillations in matter, Phys. Rev. D **17**, 2369 (1978).

[21] Y. Farzan and M. Tortola, Neutrino oscillations and non-standard interactions, Front. Phys. **6**, 10 (2018).

[22] P. S. B. Dev *et al.*, Neutrino non-standard interactions: A status report, SciPost Phys. Proc. **2**, 001 (2019).

[23] M. C. Gonzalez-Garcia, P. C. de Holanda, E. Masso, and R. Zukanovich Funchal, Probing long-range leptonic forces with solar and reactor neutrinos, J. Cosmol. Astropart. Phys. 01 (2007) 005.

[24] A. Bandyopadhyay, A. Dighe, and A. S. Joshipura, Constraints on flavor-dependent long range forces from solar neutrinos and KamLAND, Phys. Rev. D **75**, 093005 (2007).

[25] M. C. Gonzalez-Garcia, P. C. de Holanda, and R. Zukanovich Funchal, Constraints from solar and reactor neutrinos on unparticle long-range forces, J. Cosmol. Astropart. Phys. 06 (2008) 019.

[26] A. Samanta, Long-range forces: Atmospheric neutrino oscillation at a magnetized detector, J. Cosmol. Astropart. Phys. 09 (2011) 010.

[27] M. B. Wise and Y. Zhang, Lepton flavorful fifth force and depth-dependent neutrino matter interactions, J. High Energy Phys. 06 (2018) 053.

[28] K. S. Babu, G. Chauhan, and P. S. Bhupal Dev, Neutrino nonstandard interactions via light scalars in the Earth, Sun, supernovae, and the early Universe, Phys. Rev. D **101**, 095029 (2020).

[29] A. Y. Smirnov and X.-J. Xu, Wolfenstein potentials for neutrinos induced by ultra-light mediators, J. High Energy Phys. 12 (2019) 046.

[30] G. Chauhan and X.-J. Xu, Impact of the cosmic neutrino background on long-range force searches, J. High Energy Phys. 07 (2024) 255.

[31] S. Ansarifard, M. C. Gonzalez-Garcia, M. Maltoni, and J. P. Pinheiro, Solar neutrinos and leptonic spin forces, J. High Energy Phys. 07 (2024) 172.

[32] P. Coloma, M. C. Gonzalez-Garcia, and M. Maltoni, Neutrino oscillation constraints on $U(1)\prime$ models: From non-standard interactions to long-range forces, J. High Energy Phys. 01 (2021) 114; 11 (2022) 115(E).

[33] S. K. Agarwalla, M. Bustamante, M. Singh, and P. Swain, A plethora of long-range neutrino interactions probed by DUNE and T2HK, J. High Energy Phys. 09 (2024) 055.

[34] P. Mishra, R. Majhi, S. K. Pusty, M. Ghosh, and R. Mohanta, Study of long range force in P2SO and T2HKK, J. High Energy Phys. 09 (2024) 100.

[35] P. B. Denton, J. Gehrlein, and R. Pestes, *CP* -violating neutrino nonstandard interactions in long-baseline-accelerator data, Phys. Rev. Lett. **126**, 051801 (2021).

[36] I. Esteban and J. Salvado, Long range interactions in cosmology: Implications for neutrinos, J. Cosmol. Astropart. Phys. 05 (2021) 036.

[37] R. Fang, J.-H. Guo, J. Liu, and X.-P. Wang, Muon $g-2$, long-range muon spin force, and neutrino oscillations, Phys. Rev. D **110**, 035037 (2024).

[38] P. Agrawal, D. E. Kaplan, O. Kim, S. Rajendran, and M. Reig, Searching for axion forces with precision precession in storage rings, Phys. Rev. D **108**, 015017 (2023).
[39] H. Davoudiasl and R. Szafron, Muon $g-2$ and a geocentric new field, Phys. Rev. Lett. **130**, 181802 (2023).
[40] A. Ismail, W.-Y. Keung, K.-H. Tsao, and J. Unwin, Axial vector Z' and anomaly cancellation, Nucl. Phys. **B918**, 220 (2017).
[41] S. P. Mikheyev and A. Y. Smirnov, Resonance amplification of oscillations in matter and spectroscopy of solar neutrinos, Sov. J. Nucl. Phys. **42**, 913 (1985).
[42] B. Pontecorvo, Inverse beta processes and nonconservation of lepton charge, Zh. Eksp. Teor. Fiz. **34**, 247 (1957).
[43] Z. Maki, M. Nakagawa, and S. Sakata, Remarks on the unified model of elementary particles, Prog. Theor. Phys. **28**, 870 (1962).
[44] V. Brdar, J. Kopp, J. Liu, P. Prass, and X.-P. Wang, Fuzzy dark matter and nonstandard neutrino interactions, Phys. Rev. D **97**, 043001 (2018).
[45] G.-Y. Huang and N. Nath, Neutrinophilic axion-like dark matter, Eur. Phys. J. C **78**, 922 (2018).
[46] A. M. Dziewonski and D. L. Anderson, Preliminary reference earth model, Phys. Earth Planet. Interiors **25**, 297 (1981).
[47] M. Maltoni and A. Y. Smirnov, Solar neutrinos and neutrino physics, Eur. Phys. J. A **52**, 87 (2016).
[48] X.-J. Xu, Z. Wang, and S. Chen, Solar neutrino physics, Prog. Part. Nucl. Phys. **131**, 104043 (2023).
[49] N. Grevesse and A. J. Sauval, Standard solar composition, Space Sci. Rev. **85**, 161 (1998).
[50] See Supplemental Material at http://link.aps.org/supplemental/10.1103/r9p5-fxzb for a detailed comparison of oscillation probability ratios between the fifth force model and the Standard Model (SM) in reactor long-baseline (LBL) and medium-baseline (MBL) experiments. Additionally, the data analysis procedures for the KamLAND and Daya Bay reactor experiments are outlined.
[51] IceCube Collaboration, The design and performance of IceCube DeepCore, Astropart. Phys. **35**, 615 (2012).
[52] IceCube-PINGU Collaboration, Letter of intent: The precision IceCube next generation upgrade (PINGU), arXiv:1401.2046.
[53] IceCube Collaboration, The IceCube upgrade—Design and science goals, Proc. Sci. ICRC2019 (**2021**) 1031 [arXiv:1908.09441].
[54] IceCube Collaboration*, Measurement of atmospheric neutrino mixing with improved IceCube DeepCore calibration and data processing, Phys. Rev. D **108**, 012014 (2023).
[55] G. L. Fogli, E. Lisi, A. Marrone, D. Montanino, and A. Palazzo, Getting the most from the statistical analysis of solar neutrino oscillations, Phys. Rev. D **66**, 053010 (2002).
[56] D. Brzeminski, S. Das, A. Hook, and C. Ristow, Constraining vector dark matter with neutrino experiments, J. High Energy Phys. 08 (2023) 181.
[57] M. Honda, M. Sajjad Athar, T. Kajita, K. Kasahara, and S. Midorikawa, Atmospheric neutrino flux calculation using the NRLMSISE-00 atmospheric model, Phys. Rev. D **92**, 023004 (2015).
[58] T2K Collaboration, The T2K experiment, Nucl. Instrum. Methods Phys. Res., Sect. A **659**, 106 (2011).
[59] T2K Collaboration, Updated T2K measurements of muon neutrino and antineutrino disappearance using 3.6×1021 protons on target, Phys. Rev. D **108**, 072011 (2023).
[60] V. A. Ilyin, V. V. Korenkov, and D. Perret-Gallix, eds., The Super-Kamiokande detector, Nucl. Instrum. Methods Phys. Res., Sect. A **501**, 418 (2003).
[61] BOREXINO Collaboration, Comprehensive measurement of pp-chain solar neutrinos, Nature (London) **562**, 505 (2018).
[62] Super-Kamiokande Collaboration, Solar neutrino measurements using the full data period of Super-Kamiokande-IV, Phys. Rev. D **109**, 092001 (2024).
[63] KamLAND Collaboration, Constraints on θ_{13} from a three-flavor oscillation analysis of reactor antineutrinos at KamLAND, Phys. Rev. D **83**, 052002 (2011).
[64] KamLAND Collaboration, Reactor on-off antineutrino measurement with KamLAND, Phys. Rev. D **88**, 033001 (2013).
[65] Antineutrino Model. https://reactors.geoneutrinos.org.
[66] T. A. Mueller *et al.*, Improved predictions of reactor antineutrino spectra, Phys. Rev. C **83**, 054615 (2011).
[67] Daya Bay Collaboration, New measurement of antineutrino oscillation with the full detector configuration at Daya Bay, Phys. Rev. Lett. **115**, 111802 (2015).
[68] Daya Bay Collaboration, Measurement of electron antineutrino oscillation based on 1230 days of operation of the Daya Bay experiment, Phys. Rev. D **95**, 072006 (2017).
[69] Daya Bay Collaboration, Measurement of the electron antineutrino oscillation with 1958 days of operation at Daya Bay, Phys. Rev. Lett. **121**, 241805 (2018).
[70] Daya Bay Collaboration, Precision measurement of reactor antineutrino oscillation at kilometer-scale baselines by Daya Bay, Phys. Rev. Lett. **130**, 161802 (2023).
[71] P. W. Graham, S. Hacıömeroğlu, D. E. Kaplan, Z. Omarov, S. Rajendran, and Y. K. Semertzidis, Storage ring probes of dark matter and dark energy, Phys. Rev. D **103**, 055010 (2021).
[72] R. Janish and H. Ramani, Muon $g-2$ and EDM experiments as muonic dark matter detectors, Phys. Rev. D **102**, 115018 (2020).
[73] Y. Ema, T. Gao, and M. Pospelov, Muon spin force, Phys. Rev. D **110**, 075024 (2024).
[74] Muon g-2 Collaboration, Measurement of the positive muon anomalous magnetic moment to 0.46 ppm, Phys. Rev. Lett. **126**, 141801 (2021).
[75] Muon g-2 Collaboration, Measurement of the anomalous precession frequency of the muon in the Fermilab Muon $g-2$ experiment, Phys. Rev. D **103**, 072002 (2021).
[76] Muon g-2 Collaboration, Measurement of the positive muon anomalous magnetic moment to 0.20 ppm, Phys. Rev. Lett. **131**, 161802 (2023).
[77] Muon g-2 Collaboration, Detailed report on the measurement of the positive muon anomalous magnetic moment to 0.20 ppm, Phys. Rev. D **110**, 032009 (2024).

[78] Particle Data Group, Review of particle physics, Prog. Theor. Exp. Phys. **2022**, 083C01 (2022), and 2023 update.
[79] SNO Collaboration, Combined analysis of all three phases of solar neutrino data from the Sudbury Neutrino Observatory, Phys. Rev. C **88**, 025501 (2013).
[80] Super-Kamiokande Collaboration, Atmospheric neutrino oscillation analysis with external constraints in Super-Kamiokande I–IV, Phys. Rev. D **97**, 072001 (2018).
[81] Super-Kamiokande Collaboration, Atmospheric neutrino oscillation analysis with neutron tagging and an expanded fiducial volume in Super-Kamiokande I–V, Phys. Rev. D **109**, 072014 (2024).
[82] Super-Kamiokande Collaboration, Testing non-standard interactions between solar neutrinos and quarks with Super-Kamiokande, arXiv:2203.11772.